energy&fuels
article

Octane Upgrading of C_5/C_6 Light Naphtha by Layered Pressure Swing Adsorption

Patrick S. Bárcia,*[†,‡] José A. C. Silva,[‡] and Alírio E. Rodrigues[†]

[†]*Laboratory of Separation and Reaction Engineering, Departamento de Engenharia Química, Faculdade de Engenharia, Universidade do Porto, Rua do Dr. Roberto Frias, S/N 4200-465 Porto, Portugal, and* [‡]*Escola Superior de Tecnologia e Gestão, Instituto Politécnico de Bragança, Apartado 1134, 5301-857 Bragança, Portugal*

The performance of a layered pressure swing adsorption (PSA) process for the separation of high research octane number (HRON) paraffins from a C_5/C_6 light naphtha fraction is simulated with a detailed, adiabatic single column PSA model. A zeolite 5A layer is used for selective adsorption of the low RON linear paraffins, while a zeolite beta-layer is used to separate the intermediate RON 3MP from the HRON fraction. The effects of various independent process variables (zeolite 5A to zeolite beta ratio, purge to feed ratio, cycle time, operating temperature, and depressurization mode) on the key dependent process variables (product RON, HRON species recovery, HRON purity, and adsorbent productivity) are evaluated. It is demonstrated that an optimal zeolite 5A to zeolite beta ratio can improve the product average RON up to 1.0 point as compared to existing processes using zeolite 5A only. Moreover, process simulations demonstrated that increasing the operating temperature from 523 to 543 K results in an octane gain of 0.2 RON.

Introduction

Pressure swing adsorption (PSA) processes have been successfully employed for the separation of gases such as air into nitrogen and oxygen, water removal from air, hydrogen purification, and *n*-paraffins separation.[1−5] The use of pressure swing for gas separation was for the first time disclosed in a patent by Skarstrom.[6] Basically, in the Skarstrom PSA cycle, two adsorbent beds are operated by staggering a cyclic sequence of steps, such as pressurization, adsorption, blowdown, and desorption, in such a way that a nearly continuous flow of product is supplied. Afterward, many process improvements have been developed, for instance, vacuum desorption blowdown,[7] cocurrent depressurization (COD),[8] or pressure equalization.[9]

Fewer commercial applications of PSA have been realized for the separation of paraffins. One notable exception is the IsoSiv process,[10] which uses zeolite 5A to remove linear paraffins from the light straight-run (LSR) naphtha. Other variations of the IsoSiv process have been developed as part of commercial processes for the octane upgrading of the LSR naphtha; some examples are the total isomerization process (TIP) from UOP[11] and, more recently, the Ipsorb process[12,13] from Axens. These processes combine a hydroisomerization reactor for the conversion of linear molecules into branched ones and a separation unit for the recycling of low research octane number (RON) components. Most patent applications in the field are assigned to UOP[14−17] and IFP.[12] Despite the major relevance of this industrial separation process, the experimental and modeling work of Silva[18] is, as far as our knowledge goes, one of the few examples in the literature, which deepened the application of the PSA process to the separation of *n*-paraffins from a mixture containing *n*HEX, *n*PEN, and *i*PEN with zeolite 5A. The study of Silva was performed using data from a patent assigned to IFP, where a lab-scale unit operates at 573 K with a high pressure of 15 bar, a low pressure of 2 bar, and a total cycle time of 12 min. Desorption is performed by purging the adsorber with an

---

*To whom correspondence should be addressed. Telephone: +351 273 30 3191. Fax: +351 273 31 3051. E-mail: patrick.barcia@ipb.pt.

(1) Ruthven, D. M. *Principles of Adsorption and Adsorption Processes*; John Wiley: New York, 1984.

(2) Ruthven, D. M.; Farooq, S.; Knaebel, K. S. *Pressure Swing Adsorption*; VCH Publishers: New York, 1994.

(3) Suzuki, M. *Adsorption Engineering*; Kodansha: Tokyo, 1990.

(4) Wankat, P. C. *Large-Scale Adsorption and Chromatography*; CRC Press: Stoneham, MA, 1986; Vol.1.

(5) Yang, R. T. *Gas Separation by Adsorption Processes*; Butterworth Publishers: Boston, 1987.

(6) Skarstrom, C. W. Method and Apparatus for Fractionating Gaseous Mixtures by Adsorption. U.S. Patent 2,994,627, 1960.

(7) de Montgareuil, P. G.; Domine, D. Process for Separating a Binary Gaseous Mixture by Adsorption. U.S. Patent 3,155,468, 1964.

(8) Kiyonaga, K. Adsorption Separation Process. U.S. Patent 3,176,444, 1965.

(9) Marsh, W. D.; Pramuk, F. S.; Hoke, R. C.; Skarstrom, C. W. Pressure Equalization Depressuring in Heatless Adsorption. U.S. Patent 3,142,547, 1964.

(10) Cusher, N. A. UOP IsoSiv Process. In *Handbook of Petroleum Refining Processes*, 3rd ed.; Meyers, R. A., Ed.; McGraw Hill: New York, 2004b.

(11) Cusher, N. A. UOP TIP and Once-Through Zeolitic Isomerization Processes. In *Handbook of Petroleum Refining Processes*, 3rd ed.; Meyers, R. A., Ed.; McGraw Hill: New York, 2004a.

(12) Minkkinen, A.; Mank, L.; Jullian, S. Process for the Isomerization of C_5/C_6 Normal Paraffins with Recycling of Normal of Multicomponent Adsorption Beds. U.S. Patent 5,233,120, 1993.

(13) Deschamps, A.; Jullian, S. Adsorption in the Oil and Gas Industry. In *Petroleum Refining: Separation Processes*; Wauquier, J. P., Ed.; Editions Technip: Paris, 2000; Vol. 2.

(14) Holcombe, T. C. *n*-Paraffins—Isoparaffins Separation Process. U.S. Patent 4,176,053, 1979.

(15) Holcombe, T. C. Total Isomerization Process. U.S. Patent 4,210,771, 1980.

(16) Holcombe, T. C.; Sarger, T.; Volles, W. K.; Zarchy, A. S. Isomerization Process. U.S. Patent 4,929,799, 1990.

(17) Volles, W. K. Adsorptive Separation of Isopentane and di-Methyl Branched Paraffins from mono-Methyl Branched Paraffins. EU Patent 0 473 828 A1, 1992.

(18) Silva, J. A. C. Separation of n/iso-Paraffins by Adsorption Process. Ph.D. Thesis, University of Porto, 1998.

*i*PEN stream produced from a deisopentanizer (DIP) column. The huge adsorbent productivity of the Ipsorb process, 323 mmol/(min kg$_{ads}$) (productivity along the text is calculated based on the production of 22DMB, 23DMB, 3MP, *n*HEX, *i*PEN, and *n*PEN) is mainly achieved thanks to the energy-intensive DIP column and also to the detriment of the RON gain in the final product. Indeed, there is only a difference of 13 RON between the DIP feed and the adsorber product (the streams average RON is calculated considering only the contribution of 22DMB, 23DMB, 3MP, *n*HEX, *i*PEN, and *n*PEN). The ability of zeolite 5A in removing *n*-paraffins from their branched isomers is remarkable; the n/iso-alkane sorption selectivity is practically infinite.[18] However, to meet the octane targets for the modern gasoline, it is also required to separate monobranched hexanes from the isomerate mixture. For this, Volles[17] proposed an interesting variation of the PSA process by using two adsorbents, zeolite 5A and silicalite, placed as layers in the bed. The role of the silicalite layer is to reduce the concentration of LRON monobranched alkanes in the enriched fraction. The high octane gain claimed in the patent comes from the low productivity of the adsorbent, approximately 79 mmol/(min kg$_{ads}$). One of the drawbacks of this scheme is the significant amount of HRON *i*PEN recycled to the hydroisomerization reactor, due to its relatively strong adsorption in the silicalite; unlike zeolite beta, which discriminates between *i*PEN and *n*PEN,[19] in the silicalite, the adsorption strengths toward these isomers are similar at low and medium coverage.[20,21]

Despite the fast growth in the industrial applications of PSA, the design and optimization of a practical PSA scheme still remain a complex and expensive task.[22] However, with the recent development of powerful adsorption simulation packages, such as Aspen Adsim,[23] gPROMS,[24] or even the homemade simulator developed at LSRE by da Silva,[25] it becomes possible to perform efficient PSA simulations that can replace many expensive and time-consuming laboratory and pilot-scale studies.[26−29]

The aim of this work is to evaluate the effect of several process variables on the performance of a layered PSA. To achieve this task, we will make use of a rigorous model presented in a previous work by Barcia et al.[19] for the study of adsorption dynamics of C$_5$/C$_6$ naphtha fractions in a layered bed of zeolite 5A and zeolite beta. The final goal is the improvement of the actual recycle technologies for paraffins isomerization, to achieve the octane upgrading of the final product.

(19) Bárcia, P. S.; Silva, J. A. C.; Rodrigues, A. E. *Energy Fuels* **2010,** *24,* 1931–1940.
(20) Schenk, M.; Vidal, S. L.; Vlugt, T. J. H.; Smit, B.; Krishna, R. *Langmuir* **2001,** *17,* 1558–1570.
(21) Calero, S.; Smit, B.; Krishna, R. *Phys. Chem. Chem. Phys.* **2001,** *3,* 4390–4398.
(22) Sircar, S. *Ind. Eng. Chem. Res.* **2002,** *41,* 1389–1392.
(23) Aspen Technology. http://www.aspentech.com (accessed February, 2010).
(24) Process System Enterprise Limited. http://www.psenterprise.com (accessed February, 2010).
(25) da Silva, F. A. Cyclic Adsorption Processes: Application to Propane/Propylene Separation. Ph.D. Thesis, University of Porto, 1999.
(26) da Silva, F. A.; Silva, J. A. C.; Rodrigues, A. E. *Adsorption* **1999,** *5,* 229–244.
(27) Kostroski, K. P.; Wankat, P. C. *Ind. Eng. Chem. Res.* **2006,** *45,* 8117–8133.
(28) Ribeiro, A. M.; Grande, C. A.; Lopes, F. V. S.; Loureiro, J. M.; Rodrigues, A. E. *Chem. Eng. Sci.* **2008,** *63,* 5258–5273.
(29) Warmuziński, K.; Tańczyk, M. *Chem. Eng. Process.* **1997,** *36,* 59–99.

Table 1. Operating Parameters Common to All Simulations for the Layered PSA and Properties of Zeolite 5A (Taken from Silva[18]) and Zeolite beta (Taken from Barcia et al.[19])

column			
internal bed diameter (d_B)		36.6	cm
bed length (L_B)		67.7	cm
bulk porosity (ε_b)		0.35	
adsorber feed flow rate		1.6	kmol/h
adsorber feed molar composition	22DMB	3.70	mol %
	23DMB	1.85	mol %
	3MP	4.60	mol %
	*n*HEX	4.45	mol %
	*i*PEN	22.05	mol %
	*n*PEN	13.35	mol %
	H$_2$	50.00	mol %
absorber feed RON		76.9	
high pressure (P_H)		5	bar
low pressure (P_L)		1	bar

adsorbents	zeolite 5A	zeolite beta	
pellet diameter (d_p)	1.59×10^{-3}	1.59×10^{-3}	m
macropore radius (r_{pore})	8.50×10^{-8}	3.75×10^{-8}	m
adsorbent heat capacity (C_{ps})	0.865[a]	0.865[a]	kJ/kg/K
adsorbent thermal conductivity (k_s)	0.3[b]	0.3[b]	W/m/K
apparent density of pellet (ρ_p)	1.13×10^3	1.18×10^3	kg/m^3
pellet porosity (ε_p)	0.35	0.40	

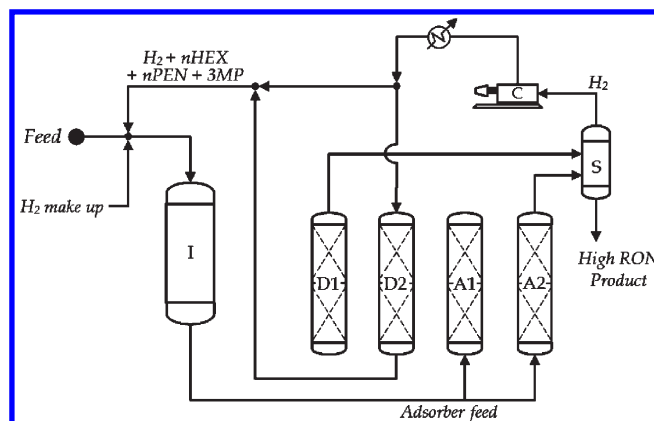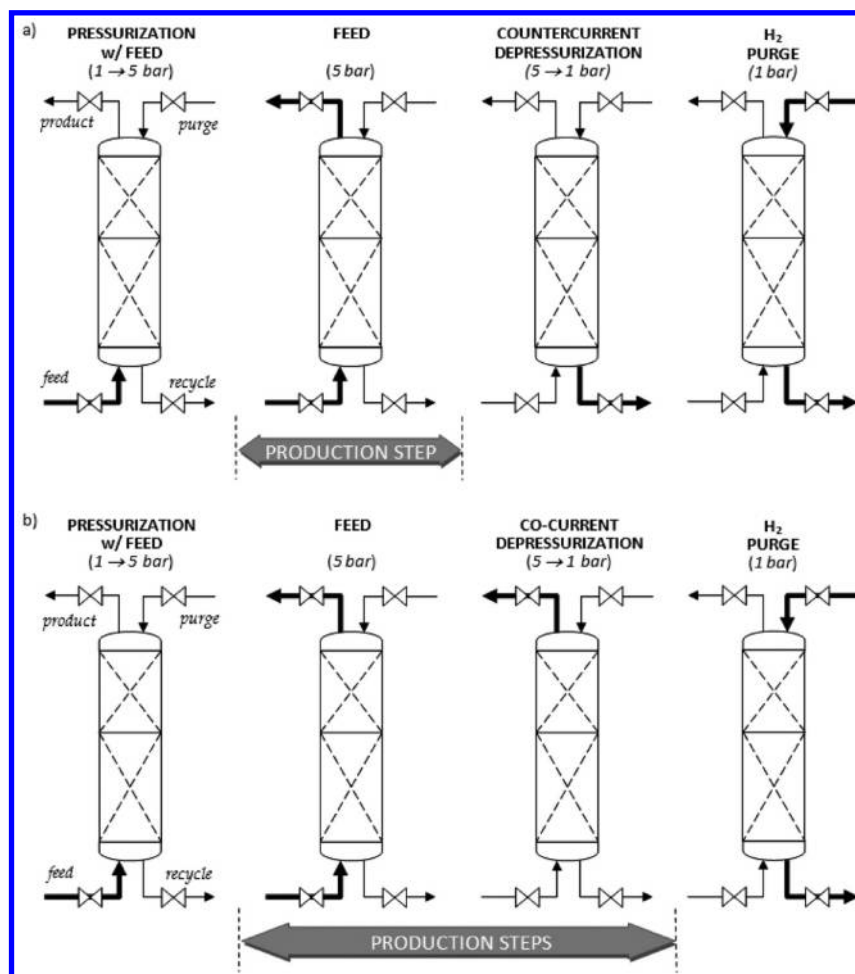[a] Taken from Boerio-Goates et al.[35] [b] Taken from Griesinger et al.[36]

Figure 1. Proposed scheme: TIP process incorporating a dual-layer PSA unit.

Study of a Single Column Layered PSA Cycle

PSA Process Description. It was demonstrated by Barcia et al.[19] that a layered fixed bed of zeolite 5A and zeolite beta can be used to produce an enriched fraction, mainly consisting of HRON molecules *i*PEN, 22DMB, and 23DMB, from a C$_5$/C$_6$ light naphtha fraction. In this work, dynamic simulation will be used to study the performance of a layered bed in a single column PSA cycle. The proposed scheme is in part based on the separation section of the TIP described by Cusher[11] but incorporates some specifications of the schemes disclosed by Minkkinen et al.[12] and Volles.[17]

The composition and flow rate of the adsorber feed are based on typical specifications from a 10000 BPD UOP commercial unit and are also given by Cusher.[11] The design of the adsorbent column is based on specifications for commercial units, described in two patents assigned to UOP. The total mass of adsorbent per bed, 54.9 tons, is given by Volles,[17] and the adsorbent column diameter, 3.66 m, is given by Holcombe[15] for a typical TIP unit. The adsorbent bed consists of a zeolite 5A layer placed at the feed end, and

Figure 2. Sequence of the four-step PSA cycle with (a) countercurrent and (b) COD modes.

Figure 3. Map of the parametric study for the process optimization.

Figure 4. Schematic diagram of the single layered bed PSA with input/output streams and gas_model blocks used for Aspen Adsim simulations.

a zeolite beta layer above the zeolite 5A layer. A bulk porosity of approximately 0.35 is typically achieved for 1/16" pellets, using the Catapac technology from Axens, which ensures homogeneous dense loading.[30] The adsorbent properties are the same as those used in a previous work.[19] The data for zeolite 5A were taken from the work of Silva.[18] The corresponding values are reported in Table 1.

To operate in the range of partial pressure covered in the adsorption equilibrium study performed by Barcia et al.[19] for C_5/C_6 isomers mixtures, it is necessary to scale down the process.
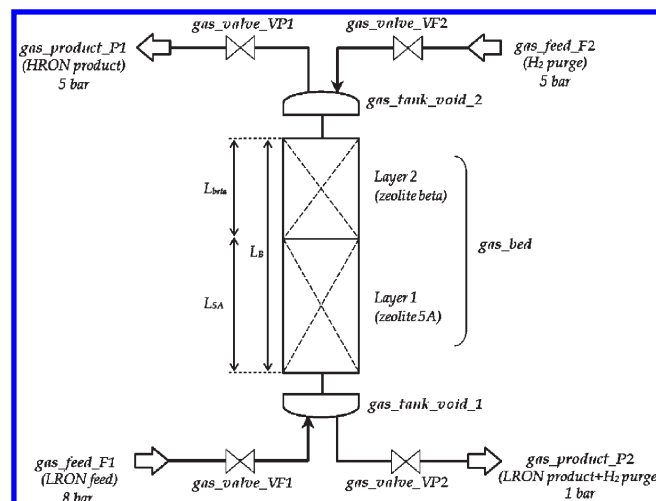
Accordingly, both the volume of the column and the adsorber feed flow rate were reduced 1000 times to keep the cycle time close to the one given by Volles.[17] The operating pressures used in the Ipsorb process for the feed step (15 bar) and the purge step (5 bar) were reduced to 5 (P_H) and 1 bar (P_L), respectively. The characteristics of the column are reported in Table 1.

(30) Axens IFP Group Technologies. http://www.axens.net (accessed February, 2010).

Table 2. Mathematical Model for the Study of the Layered Bed PSA Cycle

ideal gas law	$Py_i = RT_g c_i$
mass balance to sorbate species	$-\varepsilon_b D_{ax}\frac{\partial^2 c_i}{\partial z^2} + \frac{\partial(v_g c_i)}{\partial z} + \varepsilon_t \frac{\partial c_i}{\partial t} + \rho_b \frac{\partial \overline{q}_i}{\partial t} = 0$
axial dispersion	$D_{ax} = 0.73 D_m + \frac{v_g R_p}{\varepsilon_b (1 + 9.49 \varepsilon_b D_m / 2 v_g R_p)}$
momentum balance (Ergun's equation)	$-\frac{\partial P}{\partial z} = \frac{1.5\times10^{-3}(1-\varepsilon_b)^2}{(2R_p)^2 \varepsilon_b^3}\mu v_g + 1.75\times10^{-5} M_W \rho_g \frac{(1-\varepsilon_b)}{2R_p \varepsilon_b^3} v_g^2$
mass transfer rate to the solid	$\frac{\partial \overline{q}_i}{\partial t} = k_{MTC_i}(q_i^* - \overline{q}_i)$
LDF coefficient	$\frac{1}{k_{MTC_i}} = \frac{R_p \overline{K}_{Ki}}{3 k_{fi}} + \frac{R_p^2 \overline{K}_{Ki}}{15 \varepsilon_p D_{pi}}; \overline{K}_{Ki} = RT\frac{\rho_b}{\varepsilon_p}\frac{\partial q_i^*}{\partial p_i}; D_{pi} = [\Gamma_p(D_{K_i}^{-1} + D_{m_i}^{-1})]^{-1}; D_{K_i} = 97 r_{pore}(T/M_{Wi})^{0.5a}$
multicomponent adsorption equilibrium	zeolite 5A (Nitta model):[b]
	$\theta_i = b_i p_i \left(1 - \sum_{i=1}^N \theta_i\right)^{n_i}; \theta_i = q_i/q_i^m; b_i = b_i^0 e^{(-E_i/RT_s)}$
	zeolite beta (TSL model):
	$q_i = \sum_j \frac{q_{i,j}^m b_{i,j} p_i}{1 + \sum_{i=1}^N b_{i,j} p_i}; b_{i,j} = b_{i,j}^0 e^{(-E_{i,j}/RT_s)}$ with $j = S, Z, I$
gas phase energy balance	$-\varepsilon_b k_{gz}\frac{\partial T_g}{\partial z} + v_g C_{vg}\rho_g \frac{\partial T_g}{\partial z} + \varepsilon_t C_{vg}\rho_g \frac{\partial T_g}{\partial t} + P\frac{\partial v_g}{\partial z} + h_p a_p(T_g - T_s) = 0$
solid phase energy balance	$-k_{sz}\frac{\partial^2 T_s}{\partial z^2} + c_{ps}\rho_b \frac{\partial T_s}{\partial t} + \rho_b \sum_{i=1}^n \left(q_{sti}\frac{\partial \overline{q}_i}{\partial z}\right) - h_p a_p(T_g - T_s) = 0$
	zeolite 5A : $q_{sti} = -E_i$
	zeolite beta : $q_{sti} = \left[\sum_j \frac{-E_{i,j} q_{i,j}^m b_{i,j}}{(1 + b_{i,j} p_i)^2}\right] / \left[\sum_j \frac{q_{i,j}^m b_{i,j}}{(1 + b_{i,j} p_i)^2}\right]$
external mass transfer coefficient	$k_f = Sh_i D_{m_i}/2R_p; Sh_i = 2.0 + 1.1 Sc_i^{1/3} Re^{0.6}$
gas−solid heat transfer coefficient	$h_p = j\rho_g C_{pg} v_g Pr^{-2/3}; j = 1.66 Re^{-0.51}$ if $Re < 190$ or $j = 0.983 Re^{-0.41}$ if $Re > 190$

[a] r_{pore} is expressed in m. [b] Equilibrium data taken from Silva.

In this PSA study, it is assumed that the adsorber feed comes directly from the hydroisomerization reactor without previous H_2 separation stage. Accordingly, the temperature of the adsorber feed was fixed to 523 K, which is a typical value for hydroisomerization reactors operating with zeolite-based catalysts. A molar ratio hydrocarbon/hydrogen equal to 1 in the adsorber feed was also assumed. Barcia et al.[31] have demonstrated that the mono/dibranched selectivity in zeolite beta increases as the partial pressure decreases. Accordingly, the adsorption properties of zeolite beta might be energetically advantageous for the proposed scheme, as compared to the Ipsorb process, where the intermediate H_2 separation stage requires the subsequent vaporization of the hydrocarbon adsorber feed.

The steps sequence for the proposed scheme is similar to the one used in the Ipsorb process, with the exception of including a COD step. The COD step was implemented for the first time in an IsoSiv plant in Texas in 1961.[5] The COD allows flow out of the bed in the adsorption flow direction. The major function of the COD step is to increase the product recovery of the weak adsorptive (HRON components), which in turn enhances the purity of the strong adsorptive (LRON components) in the recycled stream. The four steps of the PSA cycle are

- Pressurization (column A1 in Figure 1): The adsorbent column, mainly filled with H_2, is pressurized with the feed mixture. The pressure in the column is raised from P_L to P_H (see also Figure 2).
- Feed (column A2 in Figure 1): The feed mixture at pressure P_H is passed through the layered bed, and a HRON-enriched fraction at pressure $\sim P_H$ is withdrawn through the product end (see Figure 2).
- COD (column D1 in Figure 1): The column is then cocurrently depressurized from P_H to P_L. Parts of the weakly adsorbed HRON molecules are desorbed from the second layer, increasing in this manner the HRON

(31) Bárcia, P. S.; Silva, J. A. C.; Rodrigues, A. E. *AIChE J.* **2007,** *53,* 1970–1981.

fraction withdrawn through the product end (see Figure 2).
- Countercurrent H_2 purge (column D2 in Figure 1): The column is countercurrently purged at P_L using a H_2 stream. The effluent mainly consisting of LRON components and H_2 is recycled to the hydroisomerization reactor (see Figure 2).

The performance of the proposed scheme will be compared with the Ipsorb PSA cycle, which uses countercurrent depressurization (CTD). For this, a CTD step will be simulated for the case where the adsorber contains only zeolite 5A. Panel a of Figure 2 shows the sequence of the four-step PSA cycle with CTD, while panel b represents the four-step PSA cycle with COD. It should be noted that the production step for a PSA cycle using CTD only comprises the feed step, while for COD, both the feed step and the depressurization steps have to be considered. Accordingly, the time of production step corresponds to the time of feed (t_{feed}) when CTD is used and to the time of feed plus the time of depressurization ($t_{feed} + t_{dpress}$) when COD is applied.

Definition of the Parametric Study. The performance of the PSA cycle with layered bed depends on several process variables, such as the fraction of zeolite 5A in the column, which is defined here as

$$L_{5A}/L_B = \frac{\text{zeolite 5A layer length}}{\text{total bed length}} \quad (1)$$

and the purge-to-feed ratio

$$P/F = \frac{\text{volume of } H_2 \text{ used in purge step}}{\text{volume of gas fed in pressurization and feed step}} \quad (2)$$

Other variables that can influence the process performances are the time of feed step (t_{feed}) and the operating temperature. To elucidate the effect of these variables, a parametric study was created, whose map and corresponding values are listed in Figure 3. First, the range of P/F ratios was simulated for the different values of L_{5A}/L_B. Then, the intermediate P/F ratio was simulated for a shorter time of

feed step. Finally, the effect of the temperature was addressed by repeating the simulations at $t_{feed} = 60$ s but for $T = 543$ K.

Process Performance Criteria. The main products of the conventional recycling schemes for isomerization processes are the monobranched and dibranched C_5/C_6 paraffins. In the process herein disclosed, the HRON molecules (*i*PEN, 22DMB, and 23DMB) are the desired products. Accordingly, the performance of the PSA cycle with COD step will be assessed by the following parameters:

$$\text{product RON} = \text{accumulated product average RON} \tag{3}$$

HRON recovery (molar basis)

$$= \frac{\text{amount of HRON withdrawn in production step}}{\text{amount of HRON fed}} \tag{4}$$

adsorbent productivity

$$= \frac{\text{amount of paraffins withdrawn in production step}}{\text{mass of adsorbent} \times \text{time of production step}} \tag{5}$$

Alternatively to the *Product RON*, octane quality can also be defined by the product purity as follows,

HRON purity (molar basis)

$$= \frac{\text{HRON withdrawn in production step}}{\text{paraffins withdrawn in production step}} \tag{6}$$

By analogy, other performance criteria relevant for the process are

$$\text{recycle RON} = \text{accumulated recycle average RON} \tag{7}$$

LRON recovery (molar basis)

$$= \frac{\text{LRON recovered in purge step}}{\text{LRON fed in pressurization and feed steps}} \tag{8}$$

LRON purity (molar basis)

$$= \frac{\text{LRON recovered in purge step}}{\text{paraffins recovered in purge step}} \tag{9}$$

Model Development

The model used to study the single column PSA cycle is implemented within Aspen Adsim 2006.5[32] using a flowsheet (see Figure 4) consisting of five different types of blocks: feed (F1 and F2), product (P1 and P2), valves (VF1, VF2, VP1, and VP2), bed (B1), and void tank (1 and 2). The behavior of each block is described by a model. The connections between blocks are used to pass information about material flow rate, composition, temperature, and pressure.

Feed Model. The feed model (F1 and F2) is used as a flowsheet inlet boundary unit, where the stream composition, pressure, and temperature are specified, while the flow rate is set as a free variable. The model simulates in this way a constant pressure reservoir with a given composition and temperature. On the basis of the feed pressure and the column inlet pressure, the feed valve unit (VF1 and VF2)

Table 3. Boundary Conditions Associated with the Four Steps of the PSA Cycle

Step 1

pressurization with feed

inlet, $z = 0$	$z = L_B$
$P\big|_{z=0} = P_{inlet}$	$v_g\big|_{z=L_B} = 0$
$D_{ax}\frac{\partial c_i}{\partial z}\big|_{z=0} = -v_g\big|_{z=0}\left(c_i\big|_{z=0^-} - c_i\big|_{z=0}\right)$	$\frac{\partial c_i}{\partial z}\big|_{z=L_B} = 0$
$k_{gz}\frac{\partial T_g}{\partial z}\big|_{z=0} = -\rho_g C_{pg} v_g\big|_{z=0}\left(T_g\big|_{z=0} - T_g\big|_{z=0}\right)$	$\frac{\partial T_g}{\partial z}\big|_{z=L_B} = 0$

Step 2

high pressure feed

inlet, $z = 0$	outlet, $z = L_B$
$v_g\big|_{z=0} = v_g\big|_{z=0^-}$	$P\big|_{z=L_B} = P_{exit}$
$D_{ax}\frac{\partial c_i}{\partial z}\big|_{z=0} = -v_g\big|_{z=0}\left(c_i\big|_{z=0^-} - c_i\big|_{z=0}\right)$	$\frac{\partial c_i}{\partial z}\big|_{z=L_B} = 0$
$k_{gz}\frac{\partial T_g}{\partial z}\big|_{z=0} = -\rho_g C_{pg} v_g\big|_{z=0}\left(T_g\big|_{z=0^-} - T_g\big|_{z=0}\right)$	$\frac{\partial T_g}{\partial z}\big|_{z=L_B} = 0$

Step 3

COD

$z = 0$	outlet, $z = L_B$
$v_g\big|_{z=0} = 0$	$P\big|_{z=L_B} = P_{exit}$
$\frac{\partial c_i}{\partial z}\big|_{z=0} = 0$	$\frac{\partial c_i}{\partial z}\big|_{z=L_B} = 0$
$\frac{\partial T_g}{\partial z}\big|_{z=0} = 0$	$\frac{\partial T_g}{\partial z}\big|_{z=L_B} = 0$

or CTD

outlet, $z = 0$	$z = L_B$
$P\big|_{z=0} = P_{exit}$	$v_g\big|_{z=L_B} = 0$
$\frac{\partial c_i}{\partial z}\big|_{z=0} = 0$	$\frac{\partial c_i}{\partial z}\big|_{z=L_B} = 0$
$\frac{\partial T_g}{\partial z}\big|_{z=0} = 0$	$\frac{\partial T_g}{\partial z}\big|_{z=L_B} = 0$

Step 4

low pressure purge (countercurrent)

outlet, $z = 0$	inlet, $z = L_B$
$P\big|_{z=0} = P_{exit}$	$v_g\big|_{z=L_B} = v_g\big|_{z=L_B^+}$
$\frac{\partial c_i}{\partial z}\big|_{z=0} = 0$	$D_{ax}\frac{\partial c_i}{\partial z}\big|_{z=L_B} = v_g\big|_{z=L_B}\left(c_i\big|_{z=L_B^+} - c_i\big|_{z=L_B}\right)$
$\frac{\partial T_g}{\partial z}\big|_{z=0} = 0$	$k_{gz}\frac{\partial T_g}{\partial z}\big|_{z=L_B} = \rho_g C_{pg} v_g\big|_{z=L_B}\left(T_g\big|_{z=L_B^+} - T_g\big|_{z=L_B}\right)$

determines the inlet flow rate. The feed pressure of units F1 and F2 was set to 8 and 5 bar, respectively.

Table 4. Operating Conditions and Process Performance of the PSA Cycles Simulated[a]

run	T (K)	DPR	t_{press} (s)	t_{feed} (s)	P/F	L_{5A}/L_B	HRON purity (%)	HRON recovery (%)	adsorbent productivity (mmol/min/kg)	product RON (−)	LRON purity (%)	LRON recovery (%)	recycle RON (−)
A	523	CTD	20	80	1.0	1.0	99.4	87.5	137.6	90.16	84.1	80.8	59.47
B	523	CTD	20	80	1.25	1.0	99.9	87.3	137.4	90.32	83.9	80.5	59.55
C	523	CTD	20	80	1.5	1.0	100.0	87.1	138.2	90.34	83.8	80.7	59.61
1	523	COD	20	80	1.0	0.0	63.4	26.0	51.0	80.51	47.2	79.5	75.79
2	523	COD	20	80	1.0	0.2	68.4	45.3	82.8	82.99	52.4	72.3	73.30
3	523	COD	20	80	1.0	0.33	74.3	50.9	85.9	85.44	56.5	76.4	71.59
4	523	COD	20	80	1.0	0.5	81.9	55.0	84.5	88.44	60.7	83.2	69.95
5	523	COD	20	80	1.0	0.67	85.2	67.3	99.6	89.77	68.1	83.5	66.81
6	523	COD	20	80	1.0	0.8	84.9	77.8	115.8	89.82	75.3	80.5	63.53
7	523	COD	20	80	1.0	1.0	81.3	98.8	154.7	88.64	97.7	69.9	53.03
8	523	COD	20	80	1.25	0.0	64.4	25.3	48.7	80.98	47.3	80.7	75.72
9	523	COD	20	80	1.25	0.2	72.9	33.9	58.1	84.74	51.0	82.5	74.11
10	523	COD	20	80	1.25	0.33	80.1	39.0	61.1	87.52	54.1	86.3	72.88
11	523	COD	20	80	1.25	0.5	86.6	46.1	66.9	89.99	58.0	89.3	71.30
12	523	COD	20	80	1.25	0.67	87.6	59.2	85.2	90.61	64.1	87.8	68.64
13	523	COD	20	80	1.25	0.8	86.8	73.2	106.5	90.49	72.2	84.4	65.00
14	523	COD	20	80	1.25	1.0	84.6	98.5	147.7	89.96	97.6	75.5	53.39
15	523	COD	20	80	1.5	0.0	67.9	21.9	40.1	82.50	47.6	85.0	75.64
16	523	COD	20	80	1.5	0.2	75.6	29.4	48.7	85.71	50.5	87.9	74.37
17	523	COD	20	80	1.5	0.33	83.6	33.9	50.9	88.63	53.1	90.1	73.41
18	523	COD	20	80	1.5	0.5	89.0	41.1	58.1	90.70	56.5	92.0	72.06
19	523	COD	20	80	1.5	0.67	88.1	56.6	81.1	90.74	63.0	89.0	69.18
20	523	COD	20	80	1.5	0.8	87.3	71.6	103.7	90.60	71.4	85.4	65.46
21	523	COD	20	80	1.5	1.0	85.5	98.6	146.4	90.26	97.7	77.0	53.46
22	523	COD	20	60	1.25	0.0	65.2	23.7	44.1	81.36	47.3	81.7	75.75
23	523	COD	20	60	1.25	0.2	75.0	29.9	48.6	85.50	50.5	85.2	74.36
24	523	COD	20	60	1.25	0.33	84.4	32.6	47.9	88.91	52.8	90.0	73.54
25	523	COD	20	60	1.25	0.5	89.5	38.9	53.5	90.88	55.6	91.6	72.35
26	523	COD	20	60	1.25	0.67	88.5	52.1	71.5	90.80	60.8	89.0	70.20
27	523	COD	20	60	1.25	0.8	87.2	67.8	96.0	90.57	68.9	85.2	66.48
28	523	COD	20	60	1.25	1.0	84.5	98.2	143.7	89.91	97.0	74.1	53.69
29	543	COD	20	60	1.25	0.0	69.7	26.3	45.7	83.40	48.6	83.1	75.17
30	543	COD	20	60	1.25	0.2	79.2	30.3	48.1	86.94	51.6	87.0	73.96
31	543	COD	20	60	1.25	0.33	87.0	34.7	49.7	89.67	53.9	91.2	73.09
32	543	COD	20	60	1.25	0.5	90.4	42.7	58.0	91.04	57.2	91.9	71.79
33	543	COD	20	60	1.25	0.67	89.1	52.6	72.7	90.92	61.3	89.9	69.99
34	543	COD	20	60	1.25	0.8	87.7	69.9	98.2	90.67	70.3	85.4	65.99
35	543	COD	20	60	1.25	1.0	84.7	98.3	143.1	89.98	97.0	74.5	53.69
32b	543	CTD	20	60	1.25	0.5	93.8	6.5	11.4	91.82	46.5	99.6	76.18

[a] Pressurization with feed, time of pressurization, and depressurization step = 20 s; DPR, depressurization with pure hydrogen in (CTD) countercurrent or (COD) cocurrent mode.

Valve Model. The flow rate through the valve is approximated by the valve model to a linear function of the pressure drop across the valve:

$$F = C_v(P_{IN} - P_{OUT}) \qquad (10)$$

where F is the molar rate through the valve and P_{IN} and P_{OUT} are the pressure upstream and downstream the valve, respectively. Equation 10 is used to calculate the value of the linear valve constant, C_v, which gives the desired molar rate for constant pressure steps. The value of C_v for a pressurization step can be estimated through the following expression

$$C_v = \frac{V_B}{RTt_{press}} \ln\left(\frac{P_{OUT}^i - P_{IN}}{P_{OUT}^f - P_{IN}}\right) \qquad (11)$$

where V_B is the effective volume of the bed, t_{press} is the time of pressurization step, P_{OUT}^i and P_{OUT}^f are the initial and final pressure in the column, respectively. Accordingly, for a depressurization step, we have

$$C_v = \frac{V_B}{RTt_{dpress}} \ln\left(\frac{P_{IN}^i - P_{OUT}}{P_{IN}^f - P_{OUT}}\right) \qquad (12)$$

where t_{dpress} is the time of depressurization step. It was assumed for all of the simulations $t_{press} = t_{dpress} = 20$ s.
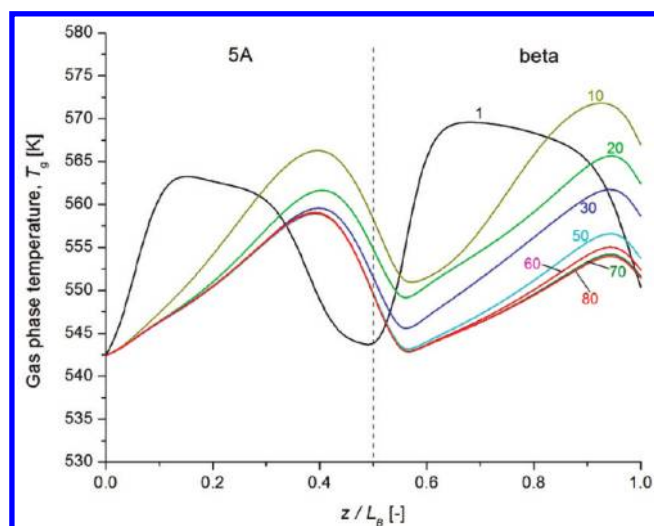

Figure 5. Evolution of gas phase temperature profile at the end of the feed step with the cycle number (run 32).

Tank Void Model. The tank void model uses well-mixed tank assumption for simulating adsorbent bed dead spaces, tanks, pressure receivers, or piping nodes. The volume of the void tanks was set to its minimum value (1×10^{-5} m^3), which
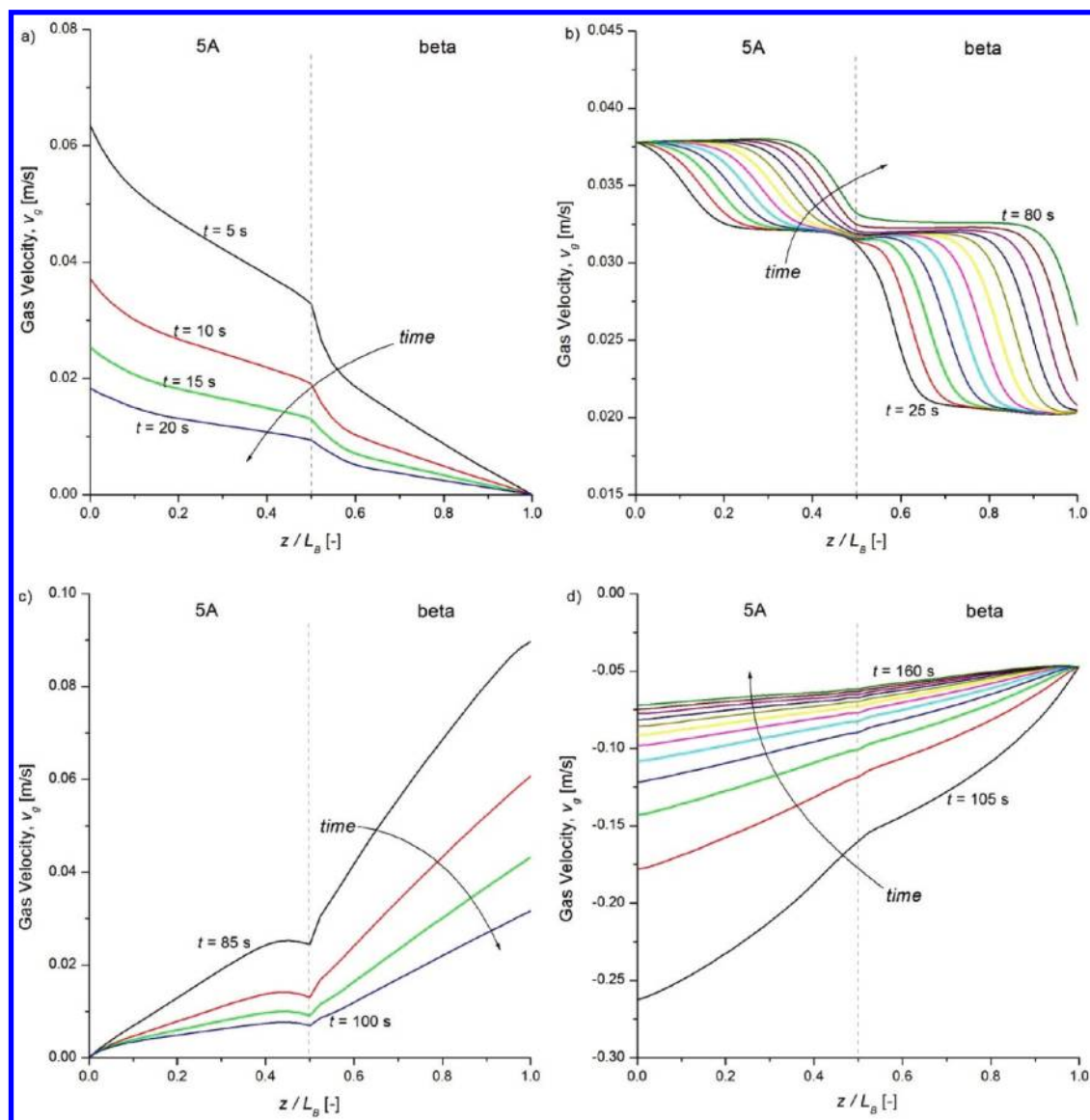
Figure 6. Evolution of the gas phase velocity profile obtained along the bed at CSS (run 32): (a) pressurization with feed, (b) adsorption, (c) COD, and (d) countercurrent purge with pure H_2.

corresponds approximately to 0.01% of the volume of the adsorption column.

Product Model. The product model (P1 and P2) is used as a flowsheet outlet boundary unit, which receives material from the flowsheet. Similarly to the feed model, the product model simulates a constant pressure reservoir, being the corresponding flow rate determined by the outlet valve unit (VP1 and VP2), based on the column outlet pressure. The pressure for unit P1 was set to 5 bar during feed step and 1 bar during depressurization step. Unit P2 was set to 1 bar pressure.

Bed Model. The typical output of the hydroisomerization reactor consists predominantly in a stream of inert gas containing 20−50 wt % alkanes in the C_5−C_6 range. Therefore, the velocity variation in the fixed bed should be considered. At the same time, because we are dealing with separation of compounds with a relatively high heat of adsorption,[19] the nonisothermal behavior in the fixed bed should be taken into account. Also, it is considered here the adiabatic condition, which is nearly approached in industrial large-size units. Accordingly, the

model used in this work is based on the following approximations:

- − The gas phase is ideal.
- − The bed operates in adiabatic conditions with gas and solid heat conduction.
- − The bed is initially filled with an inert gas in thermal equilibrium with the feed temperature.
- − Radial mass and heat dispersion are neglected, and only axial dispersion occurs.
- − The superficial velocity is related to the total pressure gradient according to Ergun's equation.
- − The main resistances to mass transfer are combined in a single lumped parameter, where the mass-transfer driving force is a linear function of the solid phase loading.
- − The adsorption equilibrium is described by the Nitta model in the zeolite 5A layer[18] and by the Trisite Langmuir model in the zeolite beta layer.[19]

The model equations are summarized in Table 2. The bed is initially filled with pure H_2, and the thermal equilibrium between the feed stream and the adsorbent column is assumed. The boundary conditions are formulated separately for each
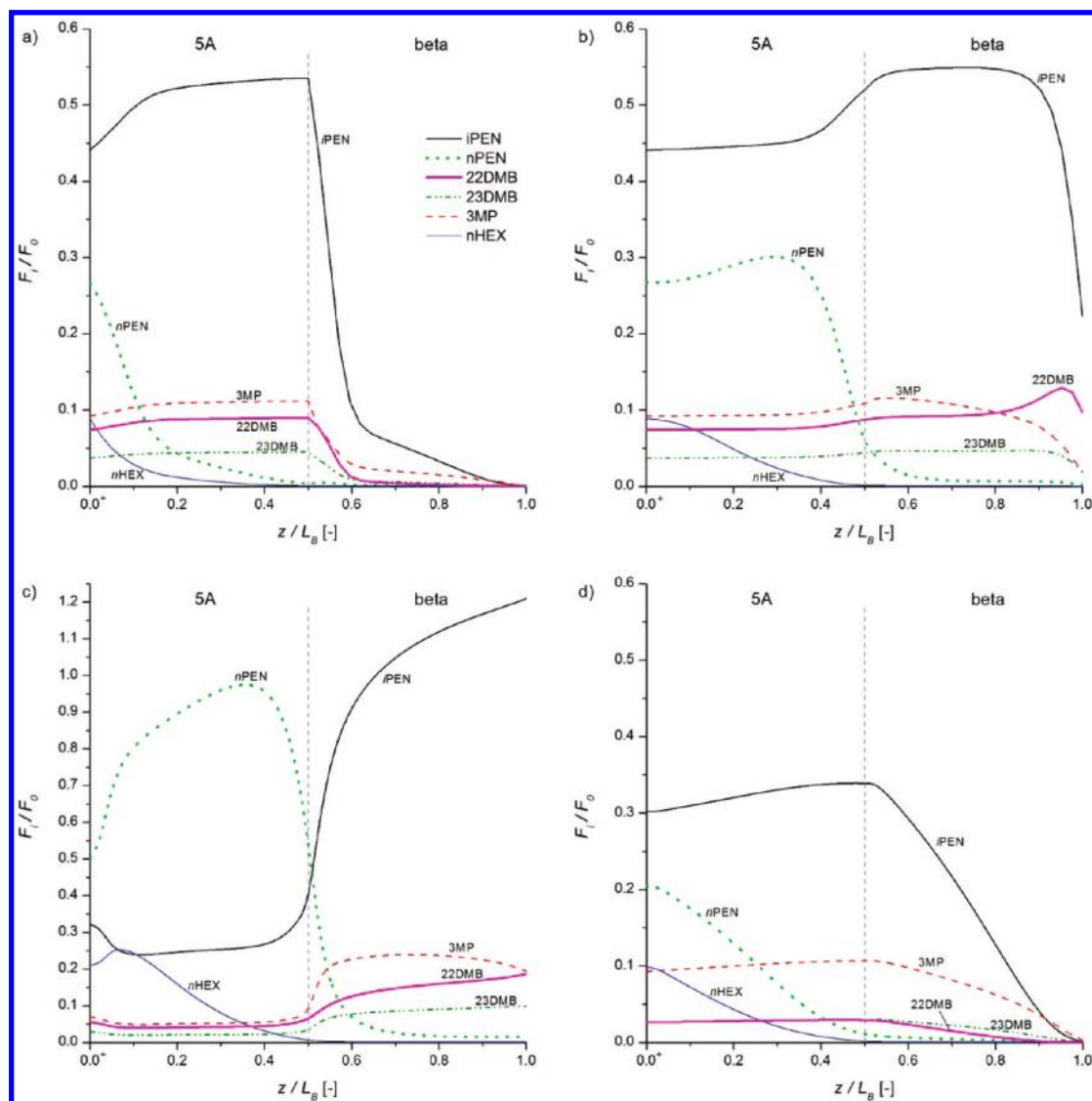
Figure 7. Gas phase concentration profile obtained along the bed at the end of each step at CSS (run 32): (a) pressurization with feed, (b) adsorption, (c) COD, and (d) countercurrent purge with pure H_2.

single PSA step. For the feed end ($z = 0$) and the product end ($z = L_B$), the boundary conditions can be written as shown in Table 3.

Numerical Methods. The set of equations was numerically solved using Aspen Adsim 2006.5. Adsim uses the method of lines[33] to solve the time-dependent partial differential equations. The spatial derivatives were discretized over a uniform grid of 42 points by the upwind differencing scheme (UDS) in conjunction with the Gear integration with variable step size of $0.01-5$ s. The physical properties of the components in the process are locally estimated through integration with the Aspen Properties database.

Results and Discussion

Layered PSA—General Dynamics. The pressure and molar rates history obtained at the column outlet during one cycle in cyclic steady state (CSS) are shown in the Supporting

Information (Figure S1). The simulation refers to run 32. The operating conditions for all of the simulations are listed in Table 4.

It can be seen from Figure S1 in the Supporting Information that the COD step causes a sharp increase of the molar flow at the bed outlet, which, in principle, breathes out a large amount of molecules from the gas phase as well as weakly adsorbed molecules from the zeolite beta layer. The process performance of a PSA cycle is only evaluated when the system reaches its CSS. However, it is important to study the behavior of the PSA cycle in the unsteady state to have a good understanding of the transport phenomena involved in the process.

The evolution of the product RON and product stream temperature is shown in Figure S2 in the Supporting Information for run 32. It can be seen from the figure that CSS is only reached after approximately 75 cycles. About 50 cycles were simulated in the work of Silva[18] for the separation of n/iso-paraffins in zeolite 5A. The main reason for this delay in achieving CSS is the stabilization of the temperature profiles within the bed, as is shown in Figure 5, where the gas phase temperature profile at the end of the feed step is plotted

(32) *Aspen Adsim 2004.1—Adsorption Reference Guide*; Aspen Technology: Cambridge, MA, 2005.
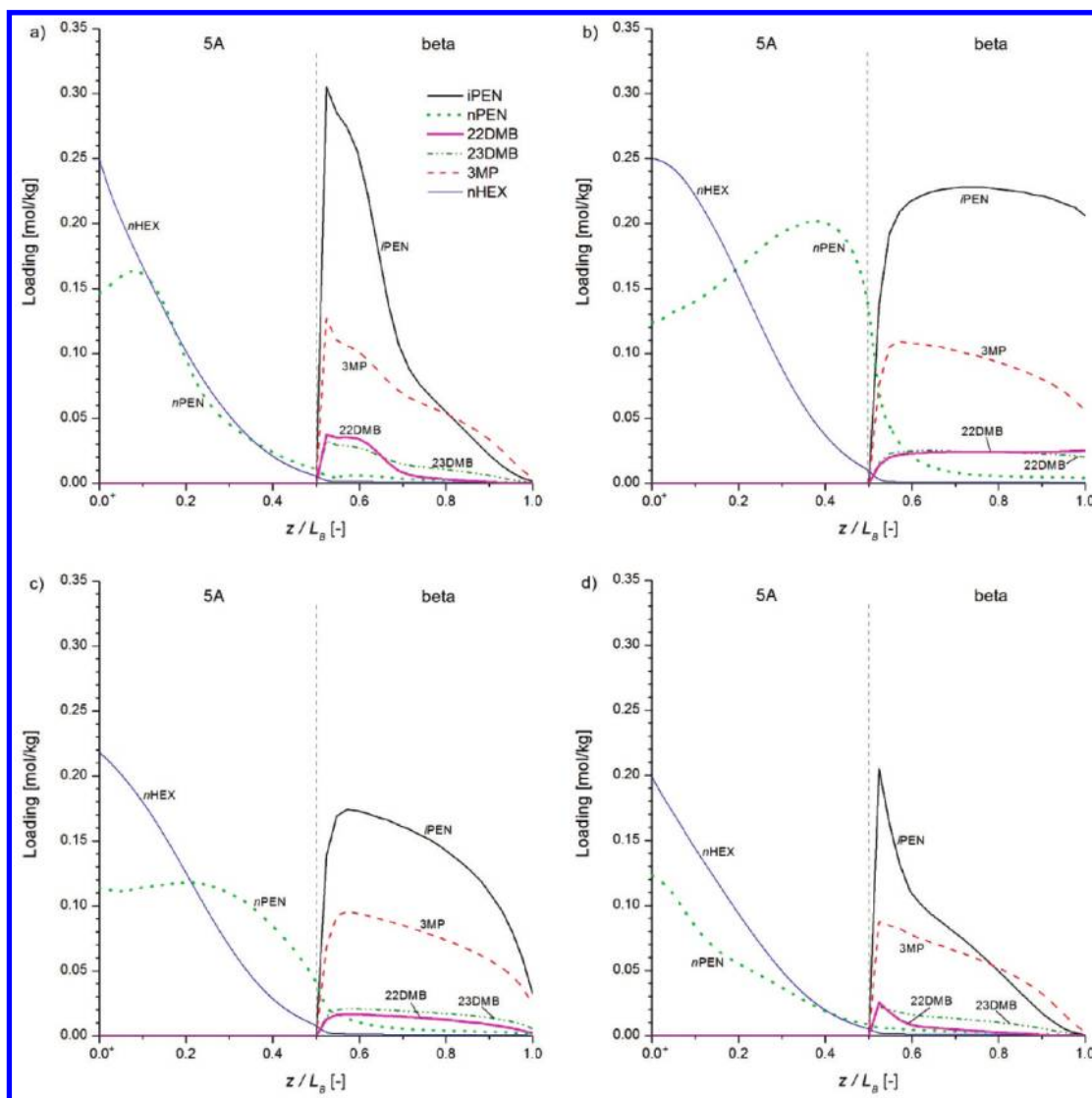(33) Schiesser, W. E. *The Numerical Method of Lines*; Academic Press: San Diego, 1991.

Figure 8. Solid phase concentration profile obtained along the bed at the end of each step at CSS (run 32): (a) pressurization with feed, (b) adsorption, (c) COD, and (d) countercurrent purge with pure H_2.

for different cycle numbers. The existence of two distinct regions in Figure 5 is explained by the difference between the adsorption properties of the adsorbent layers. It should be noted that unlike the zeolite beta layer where all of the components can be absorbed, in the zeolite 5A layer, the adsorption is restricted to the LRON molecules *n*HEX and *n*PEN. The temperature oscillation in the bed exceeds 30 K during the first cycles and progressively decreases to approximately 15 K at the CSS.

Figure S3 in the Supporting Information shows the gas phase velocity profiles at the end of the feed step for different cycle numbers (run 32). As was expected, material balance converges faster toward CSS than energy balance.

The evolution of the gas velocity profiles during each step is shown in Figure 6. The gas velocity decreases during the pressure-changing steps (panels a and c). As was stated in the boundary conditions, gas velocity is zero at the closed terminal valve of the adsorption bed (panels a and c). In the purge step, the negative velocity is because of the reversed direction of the entrance stream. As will be shown later in the text, the central plateau in the gas velocity profile of the feed step (panel b of Figure 6) is mainly due to accumulation of *i*PEN in the gas phase.
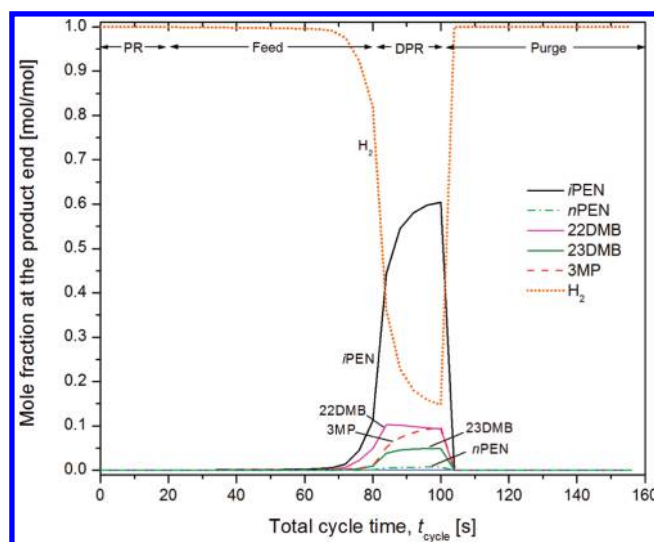

Figure 9. Molar composition at the product end as a function of the total cycle time at CSS.

Concentration Profiles in the Layered Bed at CSS. After a certain number of cycles, the PSA system runs a CSS,
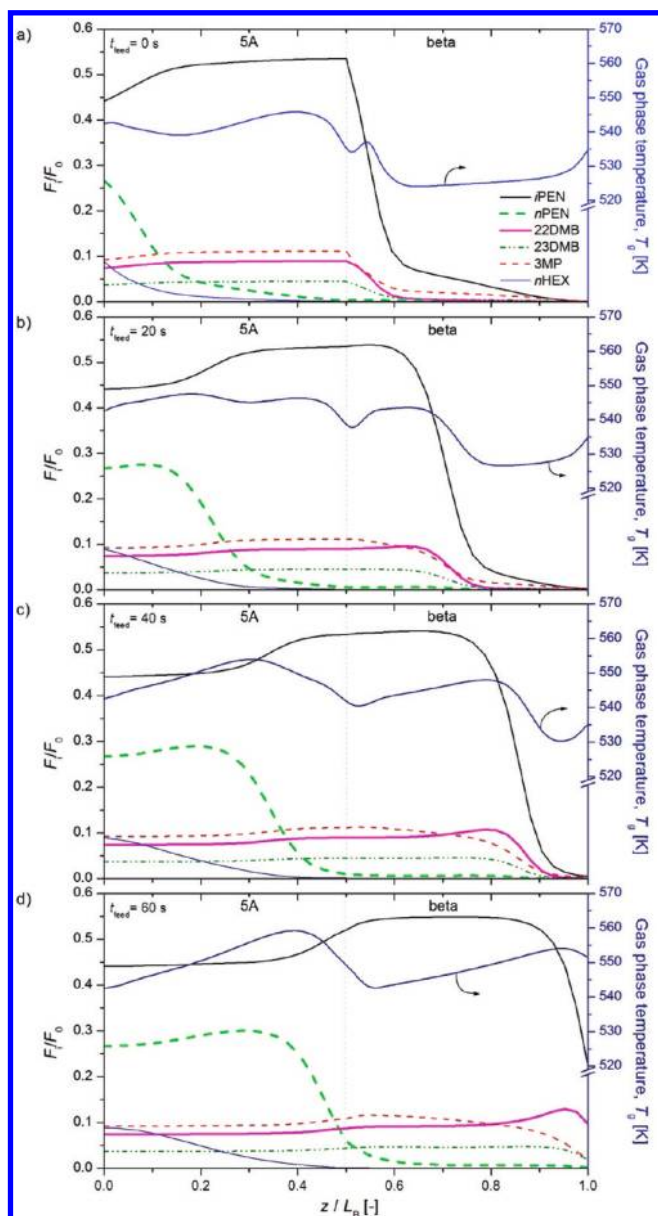
Figure 10. Evolution of the gas phase molar fraction and temperature profiles during the adsorption step at CSS (run 32): (a) $t_{feed} = 0$ s, (b) $t_{feed} = 20$ s, (c) $t_{feed} = 40$ s, and (d) $t_{feed} = 60$ s.

Figure 11. Effect of the P/F ratio on the (a) product average RON and (b) adsorbent productivity at CSS ($T = 423$ K, $t_{feed} = t_{purge} = 80$ s). Comparison between the all-zeolite 5A PSA column operating in CTD mode and the dual-layer PSA column with different zeolite 5A/zeolite beta ratio operating in COD mode.

representing normal production. Gas phase and solid phase concentration profiles at the end of each step at CSS are depicted in Figures 7 and 8, respectively, for run 32. At the end of the feed step (panel b of Figure 7), the gas phase in the zeolite beta layer is mainly composed by *i*PEN, followed by 22DMB, 3MP, and 23DMB. There is practically no *n*HEX and *n*PEN in the gas phase of this layer, because these components are strongly adsorbed in the zeolite 5A layer (panel b of Figure 8). Also, the assumption of the model in which *i*PEN, 22DMB, 23DMB, and 3MP is not adsorbed in zeolite 5A can be seen from the axial loadings in Figure 8.

Because of its high concentration in the gas phase, *i*PEN is the component more adsorbed in the zeolite beta layer. Interesting is the adsorption capacity of zeolite beta layer toward 3MP. Although the fraction of 3MP in the adsorber feed is five times lower than the *i*PEN at the end of the feed step, the loading of 3MP is practically half of the *i*PEN.
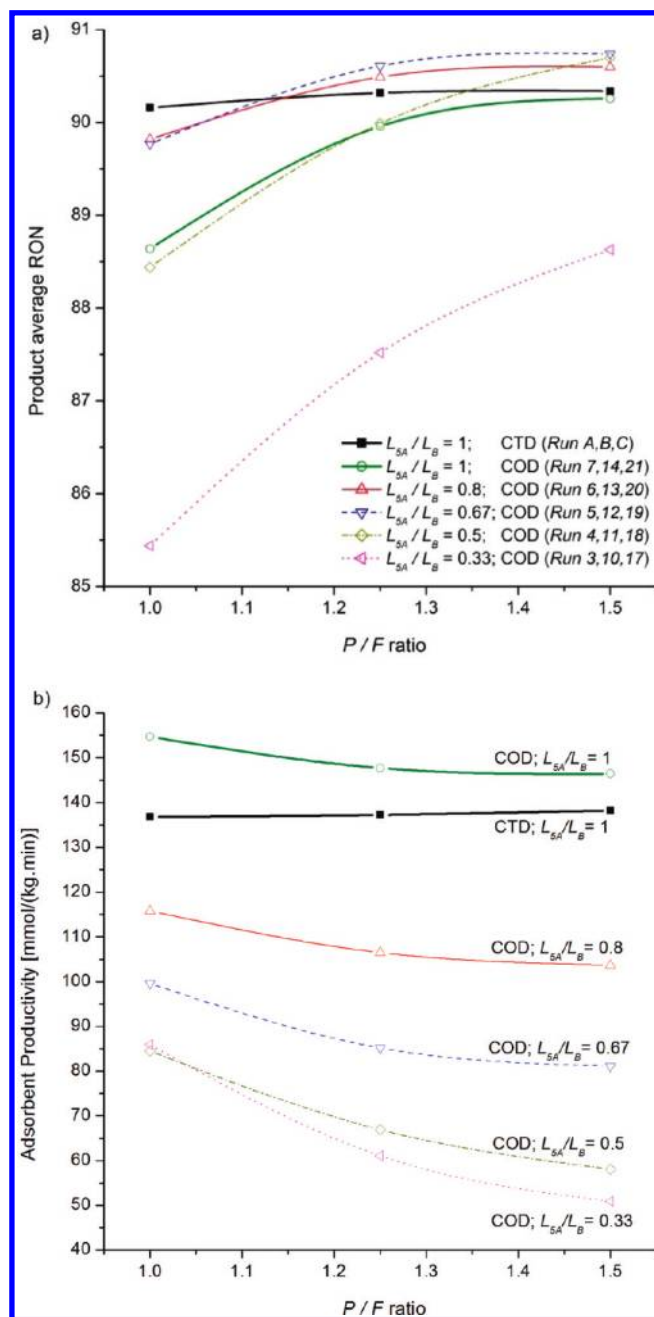
Equally remarkable is the effect of the COD step on the desorption of the weak adsorptive in the zeolite beta layer (panels b and c of Figure 8). It can be seen that the COD step leads to a significant reduction of the loading of *i*PEN and 22DMB. As a consequence, the composition of the gas that goes out of the bed during the depressurization step is enriched with HRON molecules.

The mole fractions at the product end are represented in Figure 9 for run 32 at the CSS. Only a residual amount of *n*PEN and practically no *n*HEX are recovered during production steps. As it was previously discussed, the depressurization step strongly increases the amounts of *i*PEN and 22DMB in the gas stream. At first sight, Figure 9 suggests
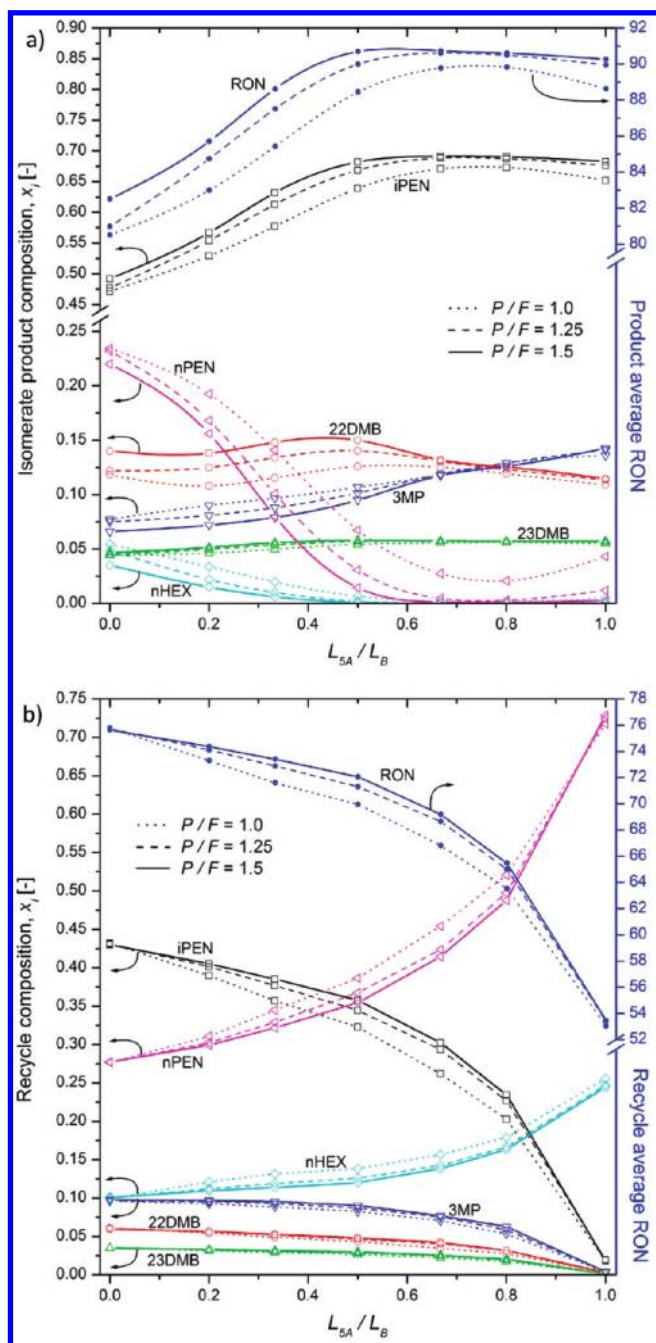
Figure 12. Effect of the *P*/*F* ratio on the composition of (a) isomerate product and (b) recycle stream and corresponding accumulated RON. The dotted lines represent runs 1−5, dashed lines represent runs 8−14, and continuous lines represent runs 15−21.

Figure 13. Effect of the cycle time on the composition of (a) isomerate product and (b) recycle stream and corresponding accumulated RON. The dashed lines represent runs 8−14, and continuous lines represent runs 22−28.

that at least four columns are required to produce a continuous stream of product.

The exothermic nature of adsorption combined with the gas flow gives rise to a temperature wave that propagates along with the concentration wave, as shown in Figure 10. In a PSA process, the temperature wave goes forward during the feed step (adsorption) and goes behind during the purge step (desorption). This temperature excursion can be useful to control the steps sequence by simply using thermocouples along the adsorption column. In Figure 10, the temperature oscillation during the feed step does not exceed 35 K. In general, the temperature excursion is greater under adiabatic conditions, which worsens the separation. Therefore, it can
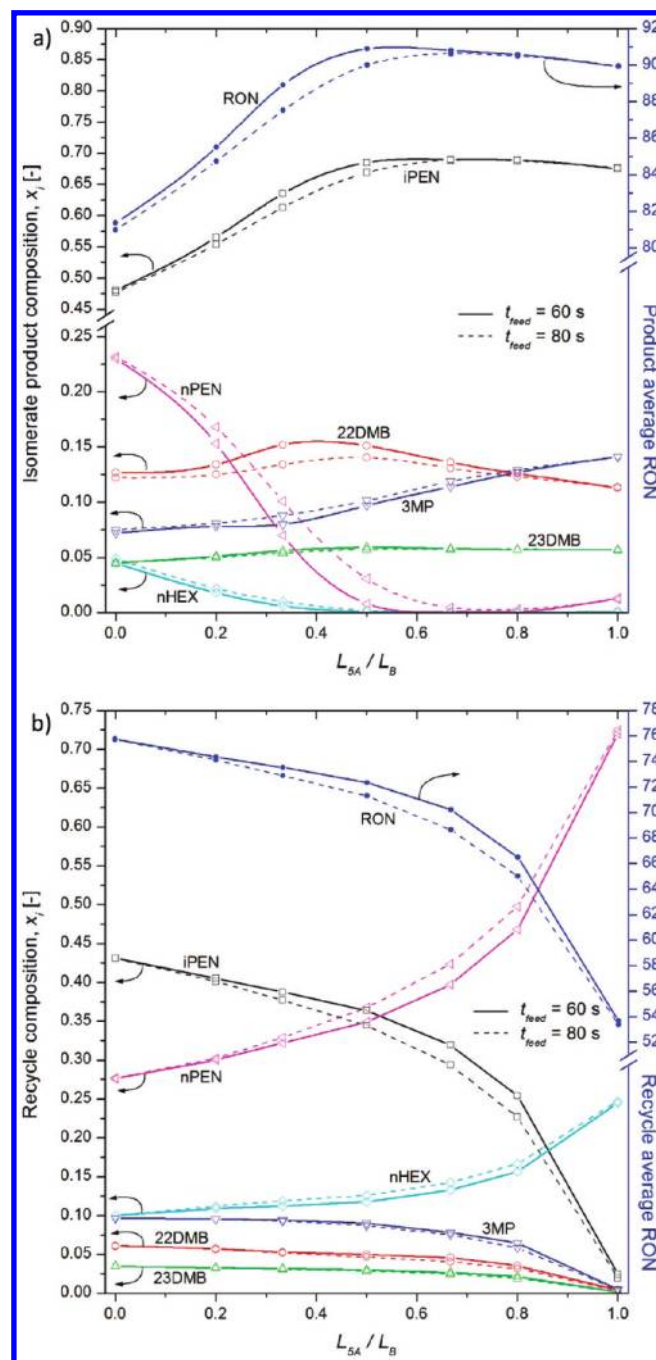
be stated that the case depicted here represents the worse scenario.

Concerning the displacement of the mass fronts during the feed step, the first remarks from Figure 10 are that *n*HEX does not cross the limit of the zeolite 5A layer, and there is just a residual fraction of *n*PEN, which reaches the zeolite beta layer. It is well-known from the equilibrium theory that for a favorable isotherm, high-concentration fronts travel faster along the adsorption column than low-concentration fronts. This fact, along with the adsorption hierarchy in zeolite beta,[19] explains why the mass front of *i*PEN travels faster during the feed step (Figure 10). The roll-up that can be observed in the concentration profile of
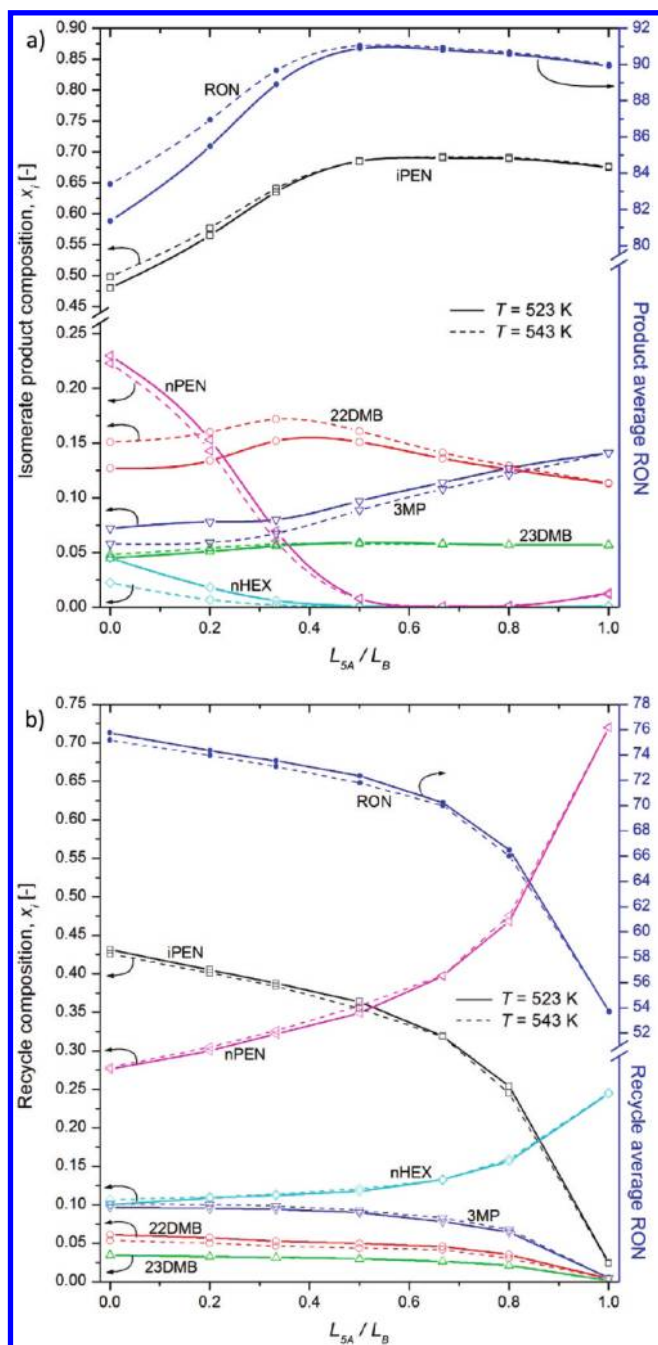
Figure 14. Effect of the operating temperature on the composition of (a) isomerate product and (b) recycle stream and corresponding accumulated product RON. The continuous lines represent runs 22–28, and dashed lines represent runs 29–35.

*i*PEN is explained by its lower affinity toward zeolite beta. The *i*PEN molecules are successively displaced from the solid phase by the more strongly adsorbed components, resulting in accumulation of *i*PEN in the gas phase.

It is interesting now to examine the propagation of the mass fronts of 3MP, 23DMB, and 22DMB during the feed step. At the beginning, the mass front of 3MP leads, but it is progressively exceeded by the 22DMB. More, at the end of the feed step, the mass front of 3MP is even overlapped by the mass front of 23DMB, which is two times more diluted than the first one. This is the evidence that the zeolite beta layer can be used as a barrier for the monobranched C_6, to reduce its concentration in the product stream.

Effect of the P/F Ratio for Different Values of L_{5A}/L_B. In practice, the volume of the purge (measured at P_L) should be equal to or greater than the volume of the feed stream (measured at P_H). The increase in volume on depressurization means that the actual H_2 molar flow (F_{purge}) required to purge the hydrocarbon in the column must be equal to or greater than one-fifth (i.e., P_L/P_H) of the molar flow of feed (F_{feed}). The case where $F_{purge} = (1/5)F_{feed}$ corresponds to a P/F ratio equal to unity.

To have a reference basis to study the performance of the proposed layered PSA unit, we first simulate cycles with a single layer of zeolite 5A and CTD step, for different P/F ratios (run A to run C), henceforth mentioned as the reference cycles. The operating conditions and process performance are in Table 4. It can be seen from runs A to C that the product RON is slightly improved as the purge is increased; however, the gain is marginal. Panel a of Figure 11 shows a comparison between the product average RON obtained with the single layer PSA cycle with CTD step and the dual layer PSA with COD step. If the faction of zeolite 5A in the dual layer (L_{5A}/L_B) is comprised in the range 0.67–0.8 and the P/F ratio is greater than 1.15, then the RON of the product will be higher than the one obtained by the reference cycle. It should be noted that the limiting cases, $L_{5A}/L_B = 0$ and $L_{5A}/L_B = 1$, correspond to a single layer of zeolite beta and a single layer of zeolite 5A, respectively. Comparing the reference cycles with the case where $L_{5A}/L_B = 1$ and the COD step is used, then it can be seen that the product RON is higher for the reference cycles. This result suggests that the COD step is not useful when the bed consists only of zeolite 5A, because the HRON molecules are not adsorbed.

In terms of productivity, it is clearly seen from panel b of Figure 11 that zeolite beta inevitably decreases the recovery of HRON components, because HRON species are also retained in the adsorbent layer. Also, it can be seen that for a all-zeolite 5A column, at a P/F ratio of 1.5, the COD step can be used to increase the productivity without significantly reducing the octane quality of product obtained.

The combined effect of P/F and L_{5A}/L_B on the composition of both product and recycle streams is shown in Figure 12. Panel a shows that when the P/F ratio is increased, the product RON is boosted. This is mainly due to a significant reduction in the concentration of *n*PEN and *n*HEX, along with an increase in the concentration of 22DMB and *i*PEN. This effect is more pronounced when the fraction of zeolite beta in the bed increases. Depending on the P/F ratio, the maximum product RON is obtained when L_{5A}/L_B ranges from 0.67 to 0.8. For instance, for $L_{5A}/L_B = 0.67$ and $P/F = 1.5$ (run 19), we obtain a final product with 90.74 RON, which represents an octane boosting of +0.40 RON comparatively to the reference cycle (run C). Less marked is the effect of the P/F ratio on the composition of the recycle stream (panel b), although a slight increase of the *i*PEN fraction is observed for intermediate values of L_{5A}/L_B.

Effect of the Cycle Time for Different Values of L_{5A}/L_B. The performance of the PSA cycle can be enhanced by the judicious choice of the cycle time. To study the effect of the cycle time, the simulations performed at 523 K and $P/F = 1.25$ (from run 8 to run 14) were repeated for a feed step (t_{feed}) of 60 s (from run 22 to run 28). It should be noted that for all of the simulations, the feed step and purge step have the same duration. The effect of the reduction of the feed step is shown in Figure 13. An enhancement of the product RON is achieved for L_{5A}/L_B in the range 0.2–0.5 (panel a).
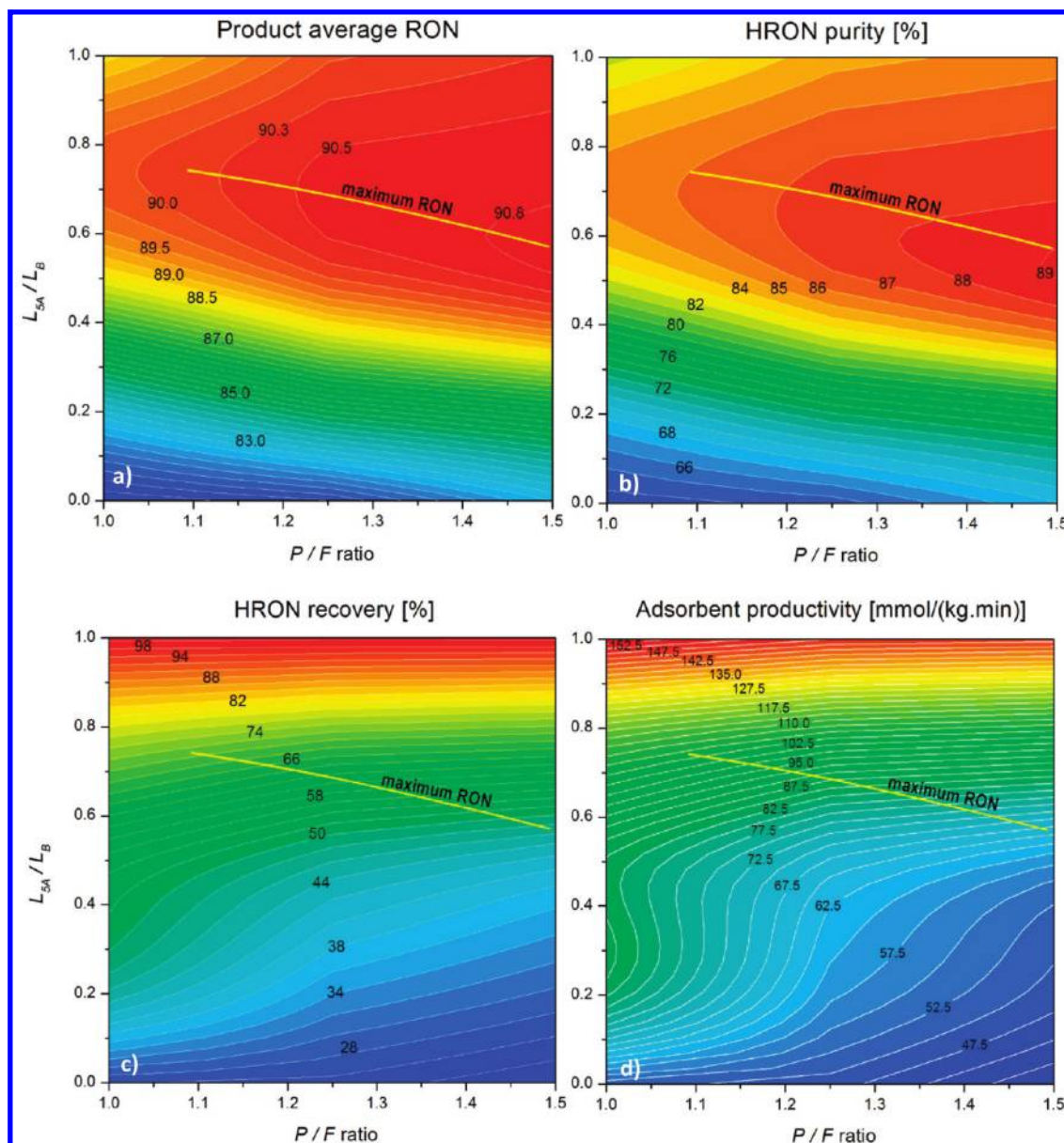
Bárcia et al.

Figure 15. General performance of the layered PSA at $T = 523$ K and $t_{press}/t_{feed} = 20/80$ s (runs 1−21) as a function of the zeolite 5A layer length and P/F ratio: (a) product average RON, (b) HRON purity, (c) recovery of HRON components, and (d) adsorbent productivity. Mass of adsorbent varying between 52.6 and 55.0 kg and production time 80 s (feed step + depressurization step).

For instance, at $L_{5A}/L_B = 0.33$, the octane gain is +1.39 RON. This improvement is mainly obtained thanks to an increase in the concentration of 22DMB and significant reduction of the concentration of *n*PEN. The maximum product RON obtained (90.88) represents an octane boosting of +0.56 RON comparatively to the reference cycle run B. The influence of the shortening of feed and purge steps on the recycle stream is shown in panel b of Figure 13.

Effect of the Temperature for Different Values of L_{5A}/L_B. It was demonstrated in a previous work by our group[19] that the rise of the temperature can have a significant impact in the separation of the C_5/C_6 isomers in zeolite beta. To study the effect of the operating temperature on the process performances, the simulations performed at 523 K, $P/F = 1.25$, and $t_{feed} = 60$ s (from run 22 to run 28) were done for an operating temperature of 543 K (from run 29 to run 35). It was assumed that the adsorber feed and the bed are at the same temperature. Nevertheless, the change in the reactor

product composition was considered to be negligible due to the small variation of the operating temperature. Figure 14 shows that a rise of 20 K in the operating temperature results in an additional increase of the product RON especially for L_{5A}/L_B lower than 0.5, that is, when the majority of the bed consists of zeolite beta. At 543 K, it is possible to reach a maximum RON of 91.04, for $L_{5A}/L_B = 0.5$. Concerning the recycle stream, it is clearly seen from panel b of Figure 14 that the temperature has no significant effect on the composition.

Effect of the Depressurization Mode. The depressurization step can be performed either cocurrently or countercurrently to the feed flow direction. The major function of the COD step in the layered PSA is to increase the recovery of the HRON molecules (weak adsorptive). However, the COD step also gives rise to the partial desorption of 3MP from the zeolite beta layer, resulting in a slight reduction of the product purity.

Table 4 (runs 32 and 32b) shows the effect of the depressurization mode on the process performances. When the process operates with CTD, there is a clear increase of the purity in both the product and the recycle streams. The octane quality of the product can be boosted up to 91.82 RON, that is, a gain of +0.78 points comparatively to the cycle operating with COD step. However, the large drawback of the CTD step is the strong reduction of the HRON recovery, almost six times less HRON recovered than the cycle operating with COD step.

General Performance of the Layered PSA Process. The simulations from run 1 to run 21 were performed at the same conditions of temperature, cycle time, and depressurization mode. Therefore, it is possible to represent the process performance in a surface graph as a function of L_{5A}/L_B and P/F. Figure 15a is for the product RON, and the line indicates the operating conditions that yield the maximum product RON. This operating line is also shown in Figure 15b, for the HRON purity of the product stream; in Figure 15c, for the recovery of HRON component; and also in Figure 15d, for the adsorbent productivity. These graphical representations allow the reader to readily find out relevant information about the process performance for a given set of operating conditions. For instance, if $L_{5A}/L_B = 0.75$ and $P/F = 1.42$, then it can be found from the surface graphs that the octane quality of the product stream will be in the range 90.6–90.7 RON, the product purity will be ∼87.5%, HRON molecules recovered in the production steps will be 68%, and adsorbent productivity will be 95 mmol/(kg$_{ads}$ min). As compared to the performance of the reference cycles run B and run C, the proposed scheme supplies an octane gain up to +0.4 RON with a reduction of approximately 30% in the adsorbent productivity.

Considering the data from Albemarle Corporation[34] for a 10000 BPSD hydroisomerization unit, the added value for an octane gain of +0.4 RON will be close to U.S. $400000 per year. Of course, the use of more adsorption beds will be required to balance the reduction of the adsorbent productivity. Nevertheless, it was seen that both the operating temperature and the cycle time can also be tuned to obtain an extra boosting in product RON.

The economic impact of power consumption for this scheme presents some major advantage when compared to conventional TIP. Indeed, the condenser for hydrogen separation, typically used after the isomerization reactor, requires subsequently a furnace to evaporate the hydrocarbon mixture prior to the PSA.[11] In the proposed scheme, hydrogen is only separated from the enriched fraction after the PSA unit and, consequently, does not requires the use of a furnace for re-evaporation (see Figure 1). Moreover, the lower the flow rate to the hydrogen separator is , the lower the energy demands. Further analysis will require the simulation of a multicolumn PSA system with equalization steps to have a more realistic representation of the actual PSA operation.

Conclusions

Simulations were performed to evaluate the performance of an adiabatic single column four step PSA cycle with a dual layer of adsorbent. The bed consists of a zeolite 5A layer to retain linear paraffins and a zeolite beta layer to separate monobranched C_6 from the enriched fraction. The proposed scheme is in part based on the separation section of the conventional TIP but incorporates some variations, such as the pressure step sequence of the Ipsorb process and a COD step. The effects of different process variables, the zeolite 5A to zeolite beta ratio, the purge to feed ratio, the cycle time, the depressurization mode, and the operating temperature on the process performances, were evaluated. The dynamic simulations demonstrate that the judicious choice of these variables can improve the octane quality of the enriched fraction comparatively to the conventional processes for the separation of *n*-paraffins. The key conclusions reached from this study are as follows:

(a) The zeolite beta layer works like a barrier for the monobranched C_6, reducing its concentration in the enriched fraction.

(b) The COD step causes the desorption of the weak adsorptive molecules from the zeolite beta layer, enriching in that manner the composition of product stream with HRON molecules.

(c) Increasing the P/F ratio boosts the octane quality of the enriched fraction. At 423 K, the maximum product RON is obtained when L_{5A}/L_B ranges from 0.67 to 0.8.

(d) For L_{5A}/L_B in the range 0.67–0.8 and a P/F ratio greater than 1.15, the product RON yield by the dual layer operating with COD will be higher than the one obtained using the single layer of zeolite 5A with CTD. For instance, keeping constant the P/F ratio, it is possible to have an octane gain of +0.26 RON with a reduction of 25% in the adsorbent productivity.

(e) At 543 K and L_{5A}/L_B in the range 0.2–0.5, the octane quality can be boosted by reducing the feed step in 20 s. This variation reduces the amount of *n*PEN in the product.

(f) Product RON can also be increased by raising the operating temperature, when the majority of the bed consists of zeolite beta. This effect results from the higher selectivity of the zeolite beta toward less branched isomers at high temperature.

(g) The COD step in the layered PSA increases the recovery of the HRON molecules. A higher product RON can be obtained using CTD step; however, with a strong reduction of the HRON recovery.

Supporting Information Available: Additional details about the general dynamics of the layered PSA simulations. This material is available free of charge via the Internet at http://pubs.acs.org.

(34) Albemarle Corporation. http://www.albemarle.com (accessed February, 2010).

(35) Boerio-Goates, J.; Stevens, R.; Hom, B. K.; Woodfield, B. F.; Piccione, P. M.; Davis, M. E.; Navrotsky, A. *J. Chem. Thermodyn.* **2002**, *34*, 205–227.

(36) Griesinger, A.; Spindler, K.; Hahne, E.; Int., J. *Heat Mass Transfer* **1999**, *42*, 4363–4374.

Nomenclature

a_p = specific particle surface per unit volume of bed (m^2$_{particle}$/m^3$_{bed}$)

b = adsorption affinity constant (bar^{-1})

b^0 = frequency factor of the affinity constant (bar^{-1})

c_i = concentration of solute i in fluid (kmol/m^3)

C_{ps} = specific heat capacity of adsorbent (kJ/kg/K)

C_{pg} = specific gas phase heat capacity at constant pressure (kJ/kmol/K)

C_{vg} = specific gas phase heat capacity at constant volume (kJ/kmol/K)

d_B = internal bed diameter (m)

d_p = particle diameter (m)

D_{ax} = axial dispersion coefficient (m^2/s)

D_K = Knudsen diffusion coefficient (m^2/s)

D_m = molecular diffusion coefficient (m^2/s)

D_p = macropore diffusion coefficient (m^2/s)

F_0 = total molar rate of adsorptive species in the feed (mol/s)

F_i = molar rate of adsorptive species i at the column outlet (mol/s)

$F_{i,0}$ = molar rate of adsorptive species i in the feed (mol/s)

h_p = gas−solid heat transfer coefficient (W/m^2/K)

ΔH_0 = heat of adsorption at zero coverage (kJ/kmol)

k_{gz} = effective axial gas phase thermal conductivity (W/m/K)

k_{sz} = effective axial solid phase thermal conductivity (W/m/K)

k_f = film mass transfer coefficient (s^{-1})

k_{MTC} = effective mass transfer coefficient (s^{-1})

$\bar{K}_K$ = dimensionless Henry's coefficient (−)

L_B = bed length (m)

L_β = zeolite beta layer length (m)

L_{5A} = zeolite 5A layer length (m)

m_{ads} = mass of adsorbent (kg)

M_W = molecular weight (kg/kmol)

p = partial pressure (bar)

P = total system pressure (bar)

Pr = Prandl number ($= \mu C_{pg}/k_g M_W$)

q_i^* = equilibrium amount adsorbed of solute i (kmol/kg$_{ads}$)

$\bar{q}_i$ = average amount of solute i adsorbed (kmol/kg$_{ads}$)

q_{st} = isosteric heat of sorption (kJ/kmol)

R_p = particle radius (m)

r_{pore} = pore radius (m)

R = universal gas constant (bar m^3/kmol/K)

Re = particle Reynolds number ($= 2R_p M_W \rho_g v_g/\mu$)

Sc = component Schmid number ($= \mu/D_m \rho_g M_W$)

Sh = component Sherwood number ($= k_f 2R_p/D_m$)

t = time (s)

T_g = gas phase temperature (K)

T_s = solid phase temperature (K)

v_g = gas phase superficial velocity (m/s)

x = molar fraction (−)

y_i = mol fraction of component i in the gas phase (−)

$y_{i,0}$ = mol fraction of component i in the hydrocarbon feed (−)

z = axial coordinate (m)

Greek Letters

ε_b = interparticle voidage (m$^3_{void}$/m$^3_{bed}$)

ε_p = intraparticle voidage (m$^3_{pore}$/m$^3_{particle}$)

ε_t = total bed voidage (m$^3_{void+pore}$/m$^3_{bed}$)

ρ_b = adsorbent bulk density (kg/m^3)

ρ_p = apparent pellet density (kg/m$^3_{pellet}$)

ρ_s = solid density of pellet (kg/m$^3_{(pellet-pore)}$)

μ = dynamic viscosity (N s/m^2)

Γ_p = tortuosity (−)